Roberto C. Callarotti (M'78–SM'83) was born in Alessandria, Italy, in 1939. He received the B.Sc.E.E. degree from the University of Texas, at Austin, in 1960, and the degrees of M.Sc.E.E., E.E., and Ph.D. from the Massachusetts Institute of Technology in 1962, 1963, and 1967, respectively.

In 1970, he was a Research Fellow at Harvard. Since 1960, he has been associated with the Instituto Venezolano de Investigaciones Científicas in Caracas, where he became Subdirector between 1980 and 1982. Since 1982, he has been President of the Fundación Instituto de Ingeniería, also in Caracas. He has worked in research and development in superconductivity, inductive measurements, amorphous materials and devices, electronic device modeling, and, recently, in microstrip analysis and device design.

Dr. Callarotti is a member of Tau Beta Pi, Eta Kappa Nu, Sigma Xi, the Venezuelan Society for the Advancement of Science, and the Advisory Committee of the Institute of Amorphous Studies.

✤

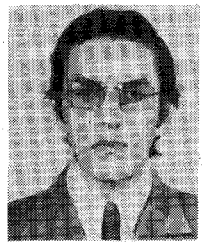

Augusto Gallo was born in Urrao, Colombia, in 1949. He received the degree of Ingeniero Electrónico from the Universidad of Antioquia, Colombia, in 1976, and the M.Sc.E.E. degree from the Instituto Venezolano de Investigaciones Científicas in 1981.

Since 1981, he has been a Professor at the Universidad del Zulia, Maracaibo, where he teaches and carries out research in microstrips.

Analysis of Wave Propagation in Anisotropic Film Waveguides with Bent Optical Axes

MASAHIRO GESHIRO, MEMBER, IEEE, YASUO KAIHARA, AND SINNOSUKE SAWA, MEMBER, IEEE

Abstract—**We present an analytical method for studying the wave propagation in anisotropic planar optical waveguides where the oblique angle between the optical axis and the propagation axis changes arbitrarily in the film surface along the propagation length. The analysis is based on the coupled-mode theory, where the coupling between a guided mode and radiation modes is regarded to be of major importance. We apply a hypothetical boundary method to quantize the continuum of radiation modes, and replace the continuously changing oblique angle by a step approximation. It is shown that these approximations do not degrade the computational accuracy. To exemplify the wave-propagation properties, we deal with a waveguide consisting of $LiNbO_3$ and let the oblique angle change linearly along the propagation length. It is found that the incident guided TE mode leaks its power primarily in a very narrow region centered on the critical oblique angle, and that TE radiation modes play an important role in the power conversion, even though they carry far less power than the TM radiation modes.**

I. Introduction

IT IS OF fundamental interest to know the guiding properties of dielectric optical waveguides composed of anisotropic, as well as isotropic, materials. Such knowledge is needed for applications to guided-wave devices for optical integrated circuits. Usually, two different approaches have been adopted in waveguide analysis. One approach is based on the eigenvalue method in which modal solutions of Maxwell's equations are determined with the help of boundary conditions provided that the waveguide is infinitely long and homogeneous along the propagation axis. Most papers on wave propagation in anisotropic waveguides using this method have dealt with purely guided modes [1]–[6]. Recently, interesting propagation characteristics of hybrid leaky modes supported by planar anisotropic waveguides or metal-diffused anisotropic waveguides have been analyzed where the optical axis of the composing material makes an oblique angle with the propagation axis in the film surface [7], [8].

The other approach is based on the coupled-mode theory [9]. It is suitable for describing the wave propagation in waveguides that are inhomogeneous along the propagation axis and/or of finite length suitable for integrated optics devices. Therefore, propagation properties obtained from it may be useful from the device-planning viewpoint. In the coupled-mode theory, power leakage of a hybrid leaky mode in an anisotropic waveguide is attributed to mode conversion between a guided mode and radiation modes of the orthogonal polarization [10]. The coupled-mode theory is always applicable to the analysis of wave propagation in anisotropic waveguides having any nondiagonal dielectric

Manuscript received January 13, 1983; revised October 19, 1983.

M. Geshiro and S. Sawa are with the Department of Electronics Engineering, Faculty of Engineering, Ehime University, 3, Bunkyo, Matsuyama, Ehime, 790 Japan.

Y. Kaihara is with Kakogawa Works, Kobe Steel, Ltd., Kanazawa, Kakogawa, Hyogo, 675-01 Japan.

0018-9480/84/0400-0339$01.00 ©1984 IEEE

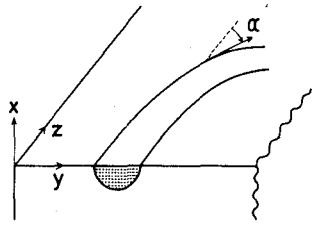

Fig. 1. Curved channel optical waveguide formed by diffusion. The optical axis of uniaxial crystalline material coincides with the z axis, and α represents a local oblique angle.

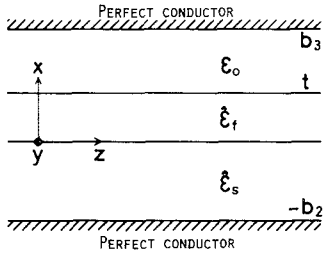

Fig. 2. Waveguide structure of the asymmetric anisotropic slab waveguide and the coordinate system used for the analysis.

tensor. For example, analyses of hybrid guided modes in rectangular waveguides, or of amplitude modulators based on the mode-conversion phenomenon due to the electrooptic effect in metal-diffused $LiNbO_3$ or $LiTaO_3$ waveguides, have been reported [5], [6], [10]–[12].

Many problems of wave propagation in various anisotropic waveguides have been studied in detail, as mentioned above. In most of the papers, however, whether diagonal or not, the dielectric tensor of the composing material does not depend on the coordinate of the propagation direction z.

Incidentally, it is difficult to avoid bends of the propagation axis in practical applications of metal-diffused waveguides composed of anisotropic materials. The oblique angle becomes a function of position along the propagation direction in a curved waveguide consisting of uniaxial crystalline materials, as shown in Fig. 1. Even in a straight waveguide, a functional dependence of the dielectric tensor on the z coordinate may be possible due to electrooptic effect, if an externally applied electric field depends on z. To the authors' knowledge, however, wave-propagation properties in such a waveguide have been scarcely studied until now.

In the present paper, we analyze the wave propagation in a straight planar waveguide composed of a uniaxial anisotropic material in which the oblique angle depends on the z coordinate. Numerical examples are given for the case that the oblique angle depends linearly on the z coordinate. It should be noted that the oblique angle in a circular bend of metal-diffused anisotropic waveguide has this functional dependence on the propagation length.

The present analysis is based on the coupled-mode theory since no normal mode exists in a nonuniform waveguide. The wave propagation is described in terms of coupled normal modes of an appropriate idealized, uniform waveguide [9]. In the present case, the coupling coefficient to a continuum of radiation modes is such a complicated function of the propagation constant, as well as of the z coordinate, that it is very difficult to obtain the exact solution of the coupled-mode equation. Therefore, we introduce two perfect conducting walls at an appropriate distance from the film surface. The continuum of radiation modes in the original waveguide becomes discrete by the additional boundary condition at the perfect conducting walls where tangential electric-field components must vanish. Secondly, the function describing the oblique angle is approximated by a succession of steps. In the limit of infinitely many steps, it is capable of approximating any arbitrary function. These approximations simplify the analytical procedure without degrading the accuracy.

II. Accuracy of the Hypothetical Boundary Method

The hypothetical boundary method has been used in the analysis of wave propagation in isotropic waveguides, but has never been applied to anisotropic problems [13]–[15]. The accuracy of the present hypothetical boundary method is discussed, and its validity is shown, in this section.

We apply the hypothetical boundary method to the problem in [10], where the hybrid leaky modes in $LiNbO_3$-planar waveguides are analyzed from the viewpoint of the coupled-mode theory. The waveguide structure under consideration is shown in Fig. 2, together with the coordinate system used for the analysis. The propagation direction of the optical wave is assumed to coincide with the z axis, and the x axis is directional normal to the film surface. Hypothetical, perfect conducting walls are located at $x = -b_2$ and $x = b_3$ parallel to the film surface; t is the film thickness. The free-space dielectric constant and dielectric tensors of the film and substrate are represented by ϵ_0, $\hat{\epsilon}_f$, and $\hat{\epsilon}_s$, respectively. The optical axis of the uniaxial material is assumed to make a certain oblique angle α, in the $y-z$ plane, with the z axis. In the waveguide coordinate system, the dielectric tensor is expressed as

$$\hat{\epsilon}_p = \epsilon_0 \begin{pmatrix} K_{xxp} & 0 & 0 \\ 0 & K_{yyp} & K_{yzp} \\ 0 & K_{zyp} & K_{zzp} \end{pmatrix} \tag{1}$$

where

$$\begin{aligned} K_{xxp} &= n_{op}^2 \\ K_{yyp} &= n_{op}^2 \cos^2\alpha + n_{ep}^2 \sin^2\alpha \\ K_{zzp} &= n_{op}^2 \sin^2\alpha + n_{ep}^2 \cos^2\alpha \\ K_{yzp} &= K_{zyp} = \left(n_{ep}^2 - n_{op}^2\right) \sin\alpha \cos\alpha. \end{aligned} \tag{2}$$

In the above equations, n_{op} and n_{ep} are the ordinary and extraordinary refractive indices of the material. The subscript p represents the film f or the substrate s.

In [10], the wave propagation is described by the coupled-mode equation in terms of normal modes of the

waveguide specified by the diagonal dielectric tensor

$$\tilde{\epsilon}_p = \epsilon_0 \begin{pmatrix} K_{xxp} & 0 & 0 \\ 0 & K_{yyp} & 0 \\ 0 & 0 & K_{zzp} \end{pmatrix} \tag{3}$$

which is obtained by putting the off-diagonal elements in (1) equal to zero. By taking account of the phase matching condition for an appropriate oblique angle, the equation is somewhat simplified as follows [10]:

$$\frac{d}{dz} g(z) = \int_{k_0}^{k_0 n_{os}} \frac{K_{zzs}}{K_{xxs}} \kappa(\beta_s) \frac{\beta_s}{\rho} r(\beta_s, z) \cdot \exp\left[j(\beta_g - \beta_s) z \right] d\beta_s \tag{4}$$

$$\frac{d}{dz} r(\beta_s, z) = -\kappa^*(\beta_s) g(z) \exp\left[j(\beta_s - \beta_g) z \right] \tag{5}$$

where g, r, β_g, and β_s represent the slowly varying complex amplitudes and the propagation constants of the TE guided and TM substrate modes, respectively. The asterisk indicates complex conjugation. ρ and $\kappa(\beta_s)$ are the transverse propagation constant and the coupling coefficient between coupled modes [10]. The propagation constants of the substrate modes belong to a continuum.

In the present analysis, the propagation constants of the substrate mode become discrete because of the additional boundary condition at the perfect conducting walls. Therefore, (4) and (5) are rewritten in the following matrix representation:

$$\frac{d}{dz} \boldsymbol{A}(z) = -j \boldsymbol{C} \cdot \boldsymbol{A}(z) \tag{6}$$

where

$$\boldsymbol{A}(z) = \begin{pmatrix} a_g(z) \\ a_{s1}(z) \\ \vdots \\ a_{sn}(z) \end{pmatrix} \tag{7}$$

and

$$\boldsymbol{C} = \begin{pmatrix} \beta_g & c_{g,s1} & & \cdots & c_{g,sn} \\ c^*_{g,s1} & \beta_{s1} & 0 & \cdots & 0 \\ & 0 & \ddots & \ddots & \vdots \\ \vdots & \vdots & \ddots & \ddots & 0 \\ c^*_{g,sn} & 0 & \cdots & 0 & \beta_{sn} \end{pmatrix}. \tag{8}$$

In the above equations, the subscripts g and si indicate the TE guided and TM substrate modes, respectively. The vector $\boldsymbol{A}$ consists of the complex amplitudes of a guided TE mode and n TM substrate modes. The matrix $\boldsymbol{C}$ is Hermitian. The coupling coefficient between the guided and substrate modes is expressed as the following overlap integral of the electric field [9]:

$$c_{g,si} = \frac{\omega}{4P} \int_{-b_2}^{b_3} \boldsymbol{E}_g^{\mathrm{TE}*} \cdot (\hat{\epsilon} - \tilde{\epsilon}) \cdot \boldsymbol{E}_{si}^{\mathrm{TM}} \, dx \tag{9}$$

where ω is the angular frequency. Mode functions and eigenvalue equations of the TE guided and TM substrate modes are expressed as follows:

$$E_y = \begin{cases} D\left\{ \sinh\gamma b_2 \cos\kappa t + \dfrac{\gamma}{\kappa} \cosh\gamma b_2 \sin\kappa t \right\} \dfrac{\sinh\left[\delta(b_3 - x)\right]}{\sinh\left[\delta(b_3 - t)\right]}, & t < x < b_3 \\ D\left\{ \sinh\gamma b_2 \cos\kappa x + \dfrac{\gamma}{\kappa} \cosh\gamma b_2 \sin\kappa x \right\}, & 0 < x < t \\ D \sinh\left[\gamma(b_2 + x)\right], & -b_2 < x < 0 \end{cases}$$

$$H_x = -\frac{\beta_g}{\omega\mu_0} E_y \qquad H_z = \frac{j}{\omega\mu_0} \frac{\partial}{\partial x} E_y \tag{10}$$

$$\kappa^2 = k_0^2 K_{yyf} - \beta_g^2$$
$$\gamma^2 = \beta_g^2 - k_0^2 K_{yys}$$
$$\delta^2 = \beta_g^2 - k_0^2 \tag{11}$$

$$\kappa^2 \tanh\left[\delta(b_3 - t)\right] \tanh\gamma b_2 \tan\kappa t - \kappa\gamma \tanh\left[\delta(b_3 - t)\right] - \kappa\delta \tanh\gamma b_2 - \gamma\delta \tan\kappa t = 0 \tag{12}$$

for the TE guided mode, where μ_0 is the free-space permeability, k_0 the free-space wavenumber, H the magnetic field, and

$$H_y = \begin{cases} \overline{D}\left\{ \cos\xi b_2 \cos\sigma t - \dfrac{\xi K_{zzf}}{\sigma K_{zzs}} \sin\xi b_2 \sin\sigma t \right\} \dfrac{\cosh\left[\Delta(b_3 - x)\right]}{\cosh\left[\Delta(b_3 - t)\right]}, & t < x < b_3 \\ \overline{D}\left\{ \cos\xi b_2 \cos\sigma x - \dfrac{\xi K_{zzf}}{\sigma K_{zzs}} \sin\xi b_2 \sin\sigma x \right\}, & 0 < x < t \\ \overline{D} \cos\left[\xi(b_2 + x)\right], & -b_2 < x < 0 \end{cases}$$

$$E_x = \frac{\beta_{si}}{\omega\epsilon_0 K_{xxp}} H_y \qquad E_z = \frac{-j}{\omega\epsilon_0 K_{zzp}} \frac{\partial}{\partial x} H_y \tag{13}$$

$$\sigma^2 = \frac{K_{zzf}}{K_{xxf}} \left(k_0^2 K_{xxf} - \beta_{si}^2 \right)$$
$$\xi^2 = \frac{K_{zzs}}{K_{xxs}} \left(k_0^2 K_{xxs} - \beta_{si}^2 \right)$$
$$\Delta^2 = \beta_{si}^2 - k_0^2 \tag{14}$$

$$\left(\frac{\sigma}{K_{zzf}} \right)^2 \coth\left[\Delta(b_3 - t)\right] \cot\xi b_2 \tan\sigma t - \frac{\sigma}{K_{zzf}} \frac{\xi}{K_{zzs}} \coth\left[\Delta(b_3 - t)\right] - \frac{\sigma\Delta}{K_{zzf}} \cot\xi b_2 - \frac{\xi\Delta}{K_{zzs}} \tan\sigma t = 0 \tag{15}$$

for the TM substrate mode. The amplitude coefficients D and $\overline{D}$ are normalized to satisfy the relation

$$P = \frac{1}{2} \int_{-b_2}^{b_3} (\boldsymbol{E} \times \boldsymbol{H}^*)_z \, dx \tag{16}$$

where P is the power carried by the mode [16].

Because C is a constant matrix, the solution of the coupled-mode equation (6) can be expressed in terms of the eigenvalue $\bar{\lambda}_\nu$ and the eigenvector U_ν of the matrix C as

$$A(z) = \sum_\nu b_\nu U_\nu \exp\left[-j\bar{\lambda}_\nu z\right] \tag{17}$$

where b_ν must be determined by a given initial condition. Now letting a TE guided mode be incident into the waveguide, we have the following initial condition at $z = 0$:

$$A(0) = \begin{pmatrix} 1 \\ 0 \\ \vdots \\ 0 \end{pmatrix}. \tag{18}$$

Substituting (18) into (17), we get

$$A(0) = U \cdot B \tag{19}$$

where the matrix U has U_ν as the νth column and the vector B consists of b_ν. Because U is a unitary matrix, we can solve (19) easily. The result is

$$B = \tilde{U} \cdot A(0) \tag{20}$$

where $\tilde{U}$ is the transposed conjugate matrix of U. Therefore, the solution of (6), satisfying the initial condition (18), is expressed as

$$A(z) = \sum_\nu u_{1\nu}^* U_\nu \exp\left[-j\bar{\lambda}_\nu z\right], \qquad z > 0 \tag{21}$$

where $u_{1\nu}$ is the element in the first row, the νth column of the matrix U. The complex amplitude for the TE guided mode is expressed as

$$a_g(z) = \sum_\nu |u_{1\nu}|^2 \exp\left[-j\bar{\lambda}_\nu z\right], \qquad z > 0. \tag{22}$$

Though the guided modes are not affected by the perfect conducting walls, substrate modes are strongly dependent on the distance b_2. The larger b_2 becomes, the more substrate modes can be supported. In the actual numerical analysis, it is not necessary to include all the substrate modes in the coupled equations (6). The influence of the location of the perfect conducting walls and the number of the coupled substrate modes that are taken into account shall be discussed later.

The waveguide parameters and the wavelength of light are assumed as $n_{of} = 2.296$, $n_{os} = 2.286$, $n_{ef} = 2.21$, $n_{es} = 2.2$, $t = 5$ μm, and λ(wavelength) $= 0.63$ μm. In this case, three TE guided modes can be supported by the waveguide. Fig. 3 shows the length dependence of the power change of the third guided TE mode (the TE_2 mode), where the oblique angle is assumed to be 15°. The ordinate represents the normalized power of the TE_2 mode $|a_g(z)|^2/|a_g(0)|^2$ and the abscissa is the normalized propagation length $k_0 z$. Solutions given by three different methods are drawn in the figure. One is the numerical solution of the coupled-mode equations (4) and (5), obtained by means of the Runge-Kutta-Gill (RKG) method. This solution can be regarded as the standard of approximating accuracy. Our solution is practically indistinguishable from the standard solution where it is assumed that $b_2 = 30t$ and

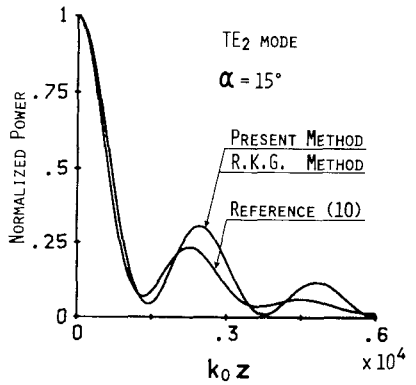

Fig. 3. Power change of the TE_2 mode due to mode conversion to TM substrate modes. The terms of the coupled TM substrate modes are 80, $b_2 = 30t$, and $b_3 = 20t$ in the present method.

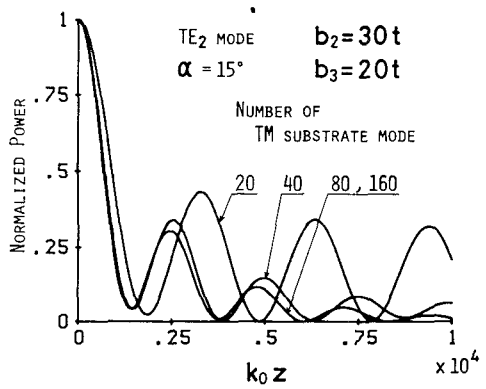

Fig 4. Power change of the TE_2 mode due to mode conversion with the number of the coupled TM substrate modes as a parameter.

$b_3 = 20t$. We have included 80 substrate modes in the calculation. Though the solution given in [10] also shows a similar tendency, its numerical values are different from the standard or our solution. We do not discuss the accuracy of the perturbation solution [17], which is not shown in the figure. Our method provides very accurate solutions for other cases of TE_0 or TE_1 mode incidence.

Next, we discuss the required number of coupled substrate modes used for the calculations. The waveguide parameters, the wavelength, and the distance between the two perfect conducting walls are assumed to have the same values as in the previous example. The incident mode is the TE_2 mode again. The dependence of the computational accuracy on the number of coupled substrate modes is illustrated in Fig. 4. In the present case, the solution converges if over 80 coupled modes are included. It is apparent, however, that the least number of the substrate modes necessary for convergence depends strongly on the location of the lower perfect conducting wall. So, for different b_2 values, we cannot consistently discuss the convergence of solution with the number of included substrate modes. Let us pay attention to the effective index in place of the number of them. Fig. 5 shows the envelope of coupling coefficients between the TE_2 mode and the coupled substrate modes. The ordinate represents the absolute value of the normalized coupling coefficient $|c_{g,st}|/k_0$ and the abscissa is the effective index β/k_0. The dashed verti-

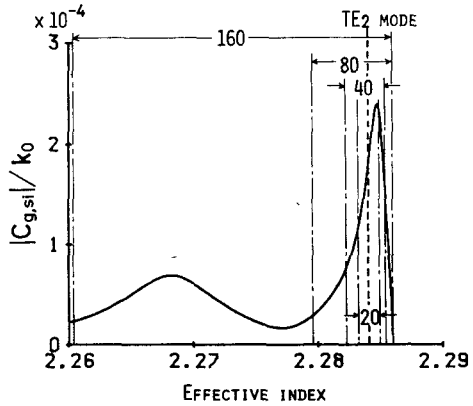

Fig. 5. The envelope of the normalized coupling coefficient between the TE_2 mode and TM substrate modes as a function of the effective index.

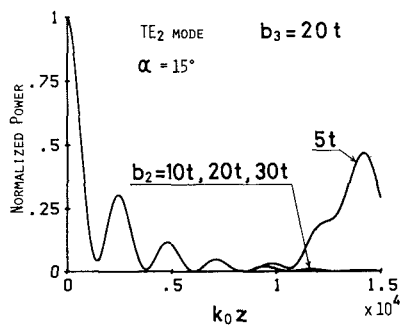

Fig. 6. Power change of the TE_2 mode due to mode conversion with the position of the lower perfect conducting wall b_2 as a parameter.

cal line indicates the effective index of the TE_2 mode. The upper limit of the effective index of the substrate mode is 2.286. The regions of effective index covered by coupled substrate modes of each case in Fig. 4 are shown in the figure. The first lobe includes almost 80 substrate modes and two lobes, the first and second, include 160 substrate modes. The solutions of these two cases are in good agreement with each other, and coincide with the standard in Fig. 4. Therefore, to get a solution of high accuracy it is necessary to use enough substrate modes to cover the main lobe. It should be noted that with increasing b_2 values, more coupled substrate modes are needed for a good approximation.

Lastly, we discuss the position of the perfect conducting walls. Because substrate modes, as well as guided modes, have evanescent fields in the cover region $t < x < b_3$, the upper wall in Fig. 2 does not affect them if it is kept at an appropriate distance from the film surface. Next, let us discuss the effect of the lower perfect conducting wall after setting the upper wall at $b_3 = 20t$. The solutions for several values of b_2 are drawn in Fig. 6. The other parameters are the same as in the previous examples. Enough coupled substrate modes are used to cover the main lobe of the coupling coefficient for each value of b_2. All curves are in complete agreement except that the curve for $b_2 = 5t$ begins to depart from the others abruptly and strikingly at the propagation length near $k_0 z = 1 \times 10^4$. The curve for $b_2 = 10t$ begins to depart at near $k_0 z = 2 \times 10^4$, which is beyond the range of the abscissa shown in the figure. This feature of the curve may be caused by radiation, which is reflected from the lower perfect conducting wall. The incident guided mode couples more strongly to the substrate mode, which most nearly matches its propagation constant. Therefore, the direction of power-leakage is approximately given by the angle satisfying

$$\cos\theta = \frac{\beta}{n_{os} k_0} \tag{23}$$

where θ is measured from the film surface to the direction of the escaping radiation and β is the propagation constant of the incident guided mode, or of the coupled substrate mode, which is phase-matched with the incident mode. The incident guided mode propagates the distance of $2b_2 \cot\theta$ along the z axis before the leakage-power comes back to the film surface again after reflection at the perfect conducting wall. When $b_2 = 5t$, the normalized propagation distance becomes $k_0 z = 1.2 \times 10^4$, which is somewhat larger than the upper limit of approximation but almost equal to it. Therefore, the applicable condition for the present method is expressed roughly as

$$k_0 z < 2 k_0 b_2 \cot\theta. \tag{24}$$

Within the region satisfying the above relation, we can expect to get a very satisfactory solution.

Incidentally, quantization of the continuum of radiation modes is also possible by truncating the substrate to have a finite thickness or assuming another substrate of finite thickness between the film and the original substrate. Identical results would be obtained by this method. With the additional layer, however, the resultant structure becomes more complicated than that of the original planar waveguide, which would be somewhat disadvantageous in application of other problems. By contrast, the perfect conducting walls are used only for simplifying the analytical procedure in the present analysis and do not alter the simplicity of the original structure.

III. Analysis of a Symmetrical Slab Waveguide with an Arbitrarily Varying Oblique Angle

The waveguide under consideration is assumed to be composed of uniaxial anisotropic materials of current interest such as $LiNbO_3$ or $LiTaO_3$. The waveguide structure and the coordinate system used for the analysis are shown in Fig. 7. The shaded portions, located parallel to the film surface in $x \geq |b|$, are perfect conducting walls where the tangential electric fields must vanish, and, in the present structure, t is the half-thickness of the film. The waveguide is symmetrical with respect to the $y-z$ plane and is uniform along the y coordinate. The z axis coincides with the propagation direction and the x axis is normal to the film surface.

Assuming that the optical axis of the material composing the film and the substrate coincides with the z axis in the region $z < 0$, we can express the dielectric tensor as fol-

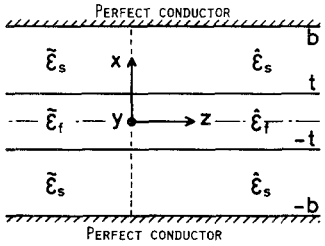

Fig. 7 Waveguide structure of the symmetric anisotropic slab waveguide and the coordinate system used for the analysis

lows:

$$\tilde{\epsilon}_p = \epsilon_0 \begin{pmatrix} n_{op}^2 & 0 & 0 \\ 0 & n_{op}^2 & 0 \\ 0 & 0 & n_{ep}^2 \end{pmatrix}. \tag{25}$$

In the region $z > 0$, if we express the oblique angle in the $y-z$ plane by an arbitrary function of z

$$\alpha = h(z) \qquad h(0) = 0 \tag{26}$$

the dielectric tensor can be represented as

$$\hat{\epsilon}_p = \epsilon_0 \begin{pmatrix} K_{xxp} & 0 & 0 \\ 0 & K_{yyp} & K_{yzp} \\ 0 & K_{zyp} & K_{zzp} \end{pmatrix} \tag{27}$$

and

$$\begin{aligned} K_{xxp} &= n_{op}^2 \\ K_{yyp} &= n_{op}^2 \cos^2\alpha + n_{ep}^2 \sin^2\alpha \\ K_{zzp} &= n_{op}^2 \sin^2\alpha + n_{ep}^2 \cos^2\alpha \\ K_{yzp} &= K_{zyp} = \left(n_{ep}^2 - n_{op}^2\right) \sin\alpha \cos\alpha. \end{aligned} \tag{28}$$

The expressions have the same form as those in the previous section, except for the functional dependence of α on z.

We are interested in the wave-propagation properties for $z > 0$ when a guided mode, whether TE or TM, propagates in the positive z direction. The wave propagation for $z > 0$ is described again by the following coupled-mode equation in terms of normal modes in $z < 0$ [9]:

$$\frac{d}{dz}\boldsymbol{A}(z) = -j\boldsymbol{C}(z)\cdot\boldsymbol{A}(z). \tag{29}$$

The vector $\boldsymbol{A}$ here consists of complex amplitudes of the guided TE and TM modes and of the TE and TM radiation modes. The matrix $\boldsymbol{C}(z)$ is Hermitian, with the following matrix element in the μth row and the νth column:

$$c_{\mu\nu} = k_{\mu\nu} + \beta_\mu \delta(\mu, \nu) \tag{30}$$

where

$$k_{\mu\nu} = \frac{\omega\epsilon_0}{4P} \int_{-b}^{b} \Delta_p E_\mu^* \cdot \hat{\delta} \cdot E_\nu \, dx \tag{31}$$

and

$$\delta(\mu, \nu) = \begin{cases} 1, & \mu = \nu \\ 0, & \mu \neq \nu \end{cases}. \tag{32}$$

We define Δ_p and $\hat{\delta}$ in (31) as

$$\Delta_p = \frac{1}{2}\left(n_{ep}^2 - n_{op}^2\right) \tag{33}$$

and

$$\hat{\delta} = \begin{pmatrix} 0 & 0 & 0 \\ 0 & \delta_{yy} & \delta_{yz} \\ 0 & \delta_{zy} & \delta_{zz} \end{pmatrix} \tag{34}$$

respectively, where

$$\begin{aligned} \delta_{yy} &= 1 - \cos 2\alpha \\ \delta_{zz} &= \cos 2\alpha - 1 \\ \delta_{yz} &= \delta_{zy} = \sin 2\alpha. \end{aligned} \tag{35}$$

Because of the symmetry of the waveguide structure, we separate the problem into two cases. In one case, the incident guided mode is of even TE (or odd TM) type, and in the other case, the odd TE (or the even TM) guided mode is incident. Let us concentrate on the case of an incident even TE guided mode. The other case can be treated in a similar manner. There exist three types of coupling: the coupling between TE modes through δ_{yy}, between TM modes through δ_{zz}, and between a TE mode and a TM mode through δ_{yz} or δ_{zy}. The coupling coefficients are expressed as

$$k_{\mu\nu}^{ee} = k_{\nu\mu}^{ee*} = \frac{\omega\epsilon_0}{4P}\delta_{yy}\int_{-b}^{b} \Delta_p E_{\mu y}^{\mathrm{TE}*} E_{\nu y}^{\mathrm{TE}} \, dx \tag{36}$$

for the TE–TE coupling, and

$$k_{\mu\nu}^{mm} = k_{\nu\mu}^{mm*} = \frac{\omega\epsilon_0}{4P}\delta_{zz}\int_{-b}^{b} \Delta_p E_{\mu z}^{\mathrm{TM}*} E_{\nu z}^{\mathrm{TM}} \, dx \tag{37}$$

for the TM–TM coupling, and

$$k_{\mu\nu}^{em} = k_{\nu\mu}^{me*} = \frac{\omega\epsilon_0}{4P}\delta_{yz}\int_{-b}^{b} \Delta_p E_{\mu y}^{\mathrm{TE}*} E_{\nu z}^{\mathrm{TM}} \, dx \tag{38}$$

for the TE–TM coupling, respectively. The rectangular components of the electric field appearing as integrands in the above integrals may be for the guided or the radiation modes. The mode functions and the eigenvalue equations are omitted here.

Now, let us apply a step approximation to (26), expressing the arbitrary oblique angle, to simplify the analysis. We divide the waveguide at $z > 0$ into consecutive sections of small distance d as shown in Fig. 8. The oblique angle is assumed to take the constant value given by the average

$$\alpha^{(i)} = \frac{1}{d}\int_{(i-1)d}^{id} h(z) \, dz, \qquad i = 1, 2, 3, \cdots \tag{39}$$

in each section. Then, we can write the coupled-mode equation in the ith section with constant coupling coefficient as

$$\frac{d}{dz}\boldsymbol{A}^{(i)}(z) = -j\boldsymbol{C}^{(i)}\cdot\boldsymbol{A}^{(i)}(z), \qquad (i-1)d < z < id. \tag{40}$$

The solution can be expressed again in terms of the eigen-

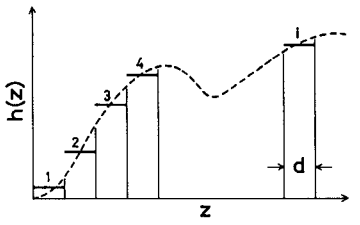

Fig. 8. Step-approximation introduced into the arbitrarily varying oblique angle.

value $\bar{\lambda}_\nu^{(i)}$ and the eigenvector $U_\nu^{(i)}$ of the matrix $C^{(i)}$ as

$$A^{(i)}(z) = \sum_\nu \tilde{U}_\nu^{(i)} \cdot A^{(i)}((i-1)d) \cdot U_\nu^{(i)} \exp\left[-j\bar{\lambda}_\nu^{(i)}\{z-(i-1)d\}\right], \quad (i-1)d < z < id \quad (41)$$

where $A^{(i)}((i-1)d)$ is the initial condition for the ith section, which is given by the following relation:

$$A^{(i)}((i-1)d) = A^{(i-1)}((i-1)d). \quad (42)$$

Therefore, we can obtain the solution at an arbitrary position $z > 0$ by successive application of (41) and (42), after getting the solution in the first section with the initial condition $A(0)$. Shorter sections increase the accuracy of the solution. The reflected waves propagating in the negative z direction are neglected in the present analysis because the index differences between successive sections are very small [18].

Lastly, we apply our method to the analysis of one concrete example. The waveguide is assumed to be composed of $LiNbO_3$. It is also assumed that the oblique angle in $z > 0$ depends linearly on the z coordinate as follows:

$$\alpha = h(z) = \frac{z}{R}, \qquad z > 0. \quad (43)$$

The above relation can be regarded as representing the oblique angle of a circularly bent waveguide with radius of curvature R.

The parameters of the waveguide structure have been chosen so that $n_{of} = 2.29$, $n_{ef} = 2.2$, $n_{os} = 2.28$, $n_{es} = 2.17$, $k_0 t = 1.6\pi$, $b/t = 30$, and $k_0 R = 1.2 \times 10^4/\pi$. Such a waveguide can support only the first guided TE and TM modes except the radiation modes, in the negative z region. Fig. 9 shows the change of modal power caused by the mode conversion in the positive z region when only the first even TE guided mode is excited in the negative z region. The coupling between TE modes may be considered to be small, so it is being neglected. The ordinate represents the normalized power of the first even TE guided mode. The oblique angle is used to represent the abscissa instead of the propagation length. The increase in the oblique angle is proportional to the propagation length. The accuracy of the approximation is illustrated in the figure with the difference of the oblique angles between two adjacent

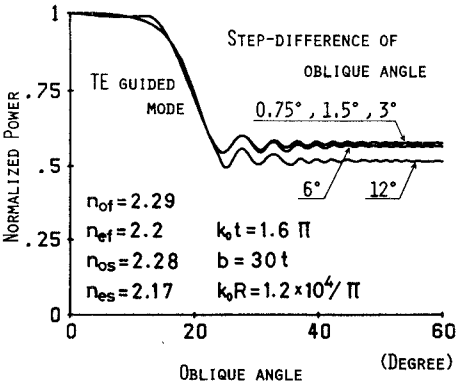

Fig. 9. Power change of the guided mode due to mode conversion with the step-difference of the oblique angle as a parameter. TE radiation modes as the coupled modes are not taken into account.

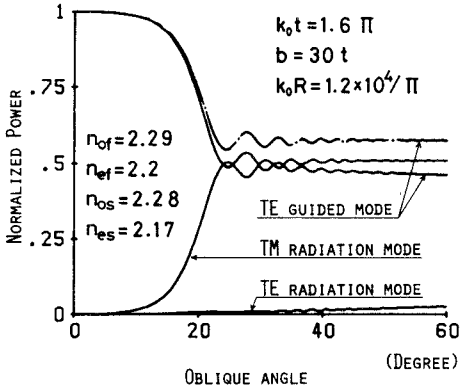

Fig. 10. Power change of the guided mode and radiation modes of both types due to mode conversion. The dashed-dotted line represents the solution obtained by neglecting TE radiation modes as the coupled modes.

sections as a parameter. It is clear that we would get solutions of considerably higher accuracy by using smaller divisions than steps of 3°. We have used 34 TM radiation modes for the numerical analysis which are covering the effective index of the TM radiation mode in the region of 2.17–2.28, and are considered to be sufficient for getting a good approximation.

Fig. 10 illustrates what happens when TE radiation modes are also included in the analysis. We included an equal number of TE and TM radiation modes for the numerical analysis. The solution obtained by neglecting the TE radiation mode is drawn again with the dashed-dotted line for comparison. The change of power of the TE guided mode in both cases shows quite similar features, except that the power, in the latter case, becomes appreciably smaller in the region of a larger oblique angle. The difference is, of course, caused by the additional TE radiation modes. Though the stored power of TE radiation modes is negligibly small, as illustrated in Fig. 10, the contribution to the power conversion between the guided TE mode and TM radiation modes cannot be neglected in the present example.

It has been pointed out that the upper limit of the critical angle at which the guided TE mode begins to leak

is defined as [7]

$$\alpha_c = \arcsin\sqrt{\frac{n_{of}^2 - n_{os}^2}{n_{of}^2 - n_{ef}^2}}\,. \tag{44}$$

We can calculate the critical angle $\alpha_c = 19.7°$ for the present example. It is found from the figures that the power of the guided TE mode decreases markedly in the narrow region of 15°–24° of the oblique angle within which the critical angle calculated from (44) is included.

Mode coupling critically depends on the phase-matching condition between the coupled modes. With the increase of the oblique angle, K_{yy} in (27) decreases according to (28), while K_{xx} remains unchanged. Since the strongest electric-field component E_y of the TE mode senses K_{yy} as the refractive index of the medium, its propagation constant decreases as the oblique angle increases. On the other hand, the propagation constant of the TM mode does not change. At any oblique angle smaller than the critical angle, there exists no TM radiation mode which is phase-matched with the guided TE mode. Therefore, the coupling to the TM radiation mode is not so significant that the power carried by the guided TE mode scarcely decreases there, as shown in Fig. 10. When the oblique angle is larger than the critical angle, the guided TE mode always matches its propagation constant with some TM radiation mode. Mode coupling, however, also depends strongly on the field overlapping between the coupled modes. The coupling coefficient given by (38) becomes an appreciable value only if both conditions are satisfied. The field of the guided mode varies according to a cosine function in the film region and decays exponentially in the surrounding region, while that of the radiation mode is expressed in terms of a standing wave throughout the entire region. The larger the oblique angle, the smaller the propagation constant of the radiation mode, which is phase-matched with the guided TE mode. For the radiation mode, the decrease of the propagation constant is accompanied by more rapid spatial oscillations in the transverse direction of the standing wave, which reduces the value of the overlap integral of the field. Therefore, the incident guided TE mode leaks its power primarily only in a very narrow region centered on the critical oblique angle as shown in Fig. 10. It would be helpful in understanding the above physical explanation to refer to [7, figs. 9 and 10].

In the present paper, the symmetric waveguide structure has been adopted for simplicity in analytical procedure. The present analysis, however, can cover the practical asymmetric metal-diffused optical waveguides as well. Numerical examples for the case of odd guided mode incidence would be applicable to them because of large asymmetry in their structure. From the present analysis, we can also get some fundamental information about channel waveguides having two-dimensional field confinement in the transverse section. In general, there exist two types of mode groups supported by such a channel waveguide as shown in Fig. 1. The mode belonging to one type is principally polarized normal to the waveguide surface, and that belonging to the other type has a principal transverse electric-field component parallel to the waveguide surface. Both types are almost TEM-like. The latter type has the same principal electric-field component as the TE mode of the slab waveguide shown in Fig. 7. Thus, the electric field of this mode senses the same refractive index as the TE mode of the slab waveguide. Therefore, the results of the present analysis will be applicable almost directly to the mode of the latter type supported by the channel waveguide.

IV. Conclusions

We have studied the wave propagation in a symmetrical, anisotropic slab waveguide consisting of uniaxial crystalline material. The direction of the optical axis may change arbitrarily along the waveguide. The analysis was based on the coupled-mode theory. We used a step function approximation for the arbitrary directional change of the optical axis, and applied the hypothetical boundary method to quantize the continuum of the radiation modes.

We first analyzed the wave propagation in the waveguide with a constant oblique angle to estimate the approximating accuracy of our method. As a result, it is found that our solution is highly accurate except for the error introduced by reflected radiation from the hypothetical boundary, which appears after the wave has traveled some distance along the waveguide. Next, we described the method used in the analysis of wave propagation in a waveguide whose optical axis changes its direction arbitrarily. A waveguide with linear oblique angle change was analyzed as a concrete example.

As a result, it is found that the guided TE mode leaks its power predominantly in a very narrow region around the critical oblique angle, and that TE radiation modes play an important role in the power conversion, though the amount of power carried by them is much smaller than that of TM radiation modes.

References

[1] Y. Satomura, M. Matsuhara, and N. Kumagai, "Analysis of electromagnetic-wave modes in anisotropic slab waveguide," *IEEE Trans. Microwave Theory Tech.*, vol. MTT-22, pp. 86–92, Feb. 1974.

[2] W. K. Burns and J. Warner, "Mode dispersion in uniaxial optical waveguides," *J. Opt. Soc. Amer.*, vol. 64, pp. 441–446, Apr. 1974.

[3] V. Ramaswamy, "Propagation in asymmetric anisotropic film waveguides," *Appl. Opt.*, vol. 13, pp. 1363–1371, June 1974.

[4] D. Marcuse, "Modes of a symmetric slab optical waveguide in birefringent media, Part I: Optical axis not in plane of slab," *IEEE J. Quantum Electron.*, vol. QE-14, pp. 736–741, Oct. 1978.

[5] R. A. Steinberg and T. G. Giallorenzi, "Modal fields of anisotropic channel waveguides," *J. Opt. Soc. Amer.*, vol. 67, pp. 523–533, Apr. 1977.

[6] M. Ohtaka, "Analysis of the guided modes in the anisotropic dielectric rectangular waveguides," *Trans. IECE Japan*, vol. J64-C, pp. 674–681, Oct. 1981.

[7] D. Marcuse and I. P. Kaminow, "Modes of a symmetric slab optical waveguide in birefringent media. Part II: Slab with coplanar optical axis," *IEEE J. Quantum Electron.*, vol. QE-15, pp. 92–101, Feb. 1979.

[8] K. Yamanouchi, T. Kamiya, and K. Shibayama, "New leaky surface waves in anisotropic metal-diffused optical waveguides," *IEEE Trans. Microwave Theory Tech.*, vol. MTT-26, pp. 298–305, Apr. 1978.

[9] D. Marcuse, "Coupled-mode theory for anisotropic optical wave-

guides," *Bell Syst. Tech. J.*, vol. 54, pp. 985–995, July–Aug. 1975.
[10] Y. Okamura, S. Yamamoto, and T. Makimoto, "Guided-to-radiation mode conversion in $LiNbO_3$ planar waveguides—Coupled-mode analysis and application to intensity modulator," *Trans. IECE Japan*, vol. J61-C, pp. 579–586, Sept. 1978.
[11] D. Marcuse, "Electrooptic coupling between TE and TM modes in anisotropic slabs," *IEEE J. Quantum Electron.*, vol. QE-11, pp. 759–767, Sept. 1975.
[12] M. Nakajima, H. Onodera, I. Awai, and J. Ikenoue, "High-efficiency light modulator using guided-to-radiation mode coupling: A proposal," *Appl. Opt.*, vol. 20, pp. 2439–2443, July 1981.
[13] D. Marcuse, "Theory of the single-material fiber," *Bell Syst. Tech. J.*, vol. 53, pp. 1619–1641, Oct. 1974.
[14] G. H. Brook and M. M. Z. Kharadly, "Step discontinuities on dielectric waveguides," *Electron. Lett.*, vol. 12, pp. 473–475, Sept. 1976.
[15] S. Sawa, K. Ono, and M. Sakuma, "Analysis of tapered optical slab waveguides with hypothetical boundaries," *Electron. Commun. Japan*, vol. 63, pp. 99–106, Feb. 1980.
[16] D. Marcuse, *Light Transmission Optics*. New York: Van Nostrand Reinhold, 1972, p. 308, eq. (8.3–17) or p. 312, eq. (8.3–39).
[17] D. Marcuse, *Theory of Dielectric Optical Waveguides*. New York and London: Academic Press, 1974, pp. 111–116.
[18] J. A. Stratton, *Electromagnetic Theory*. New York and London: McGraw-Hill, 1941, p. 496, eq. (32).

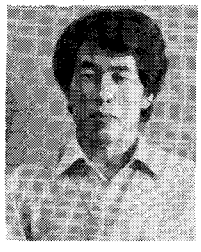

Masahiro Geshiro (S'75–M'78) was born in Osaka, Japan, on August 28, 1949. He received the B.E., M.E., and Ph.D. degrees in electrical communication engineering in 1973, 1975, and 1978, respectively, all from Osaka University, Osaka, Japan.

He is currently an Associate Professor of the Department of Electronics Engineering at Ehime University, Matsuyama, Japan. He has been engaged in research on optical transmission lines and optical integrated circuits.

Dr. Geshiro is a member of the Institute of Electronics and Communication Engineers of Japan.

Yasuo Kaihara received the B.E. and M.E. degrees in electronics engineering from Ehime University, Matsuyama, Japan, in 1981 and 1983, respectively. His main research interest was concerned with dielectric optical waveguides.

He is presently with Kakogawa Works, Kobe Steel, Ltd., Hyogo, Japan.

Mr. Kaihara is a member of the Institute of Electronics and Communication Engineers of Japan.

Sinnuosuke Sawa (M'72) was born in Osaka, Japan, on October, 23, 1938. He received the B.E. degree in electrical engineering from the University of Osaka Prefecture, Osaka, Japan, in 1962, and the M.E. and Ph.D. degrees, both in electrical communication engineering, from Osaka University, Osaka, Japan, in 1967 and 1970, respectively.

From 1962 to 1964, he worked in industry for the Mitsubishi Electric Corporation, where he was engaged in ignitron manufacture and vacuum switch development at the Kyoto Plant of the Corporation. From 1970 to 1976, he was an Associate Professor of Electronics Engineering at Ehime University. Since 1976, he has been a Professor of Electronics Engineering at Ehime University, Matsuyama, Japan, where he is engaged in research and education in electromagnetic theory, electromagnetic wave engineering, optical waveguides, and optical integrated circuits.

Dr. Sawa is a member of the Institute of Electronics and Communication Engineers of Japan, the Institute of Electrical Engineers of Japan, and the Laser Society of Japan.